Elastic forward scattering in the cuprate superconducting state

L. Zhu,[1] P. J. Hirschfeld,[1] and D. J. Scalapino[2]
[1]*Department of Physics, University of Florida, Gainesville, Florida 32611, USA*
[2]*Department of Physics, University of California, Santa Barbara, California 93106, USA*
(Received 13 June 2004; published 3 December 2004)

We investigate the effect of elastic forward scattering on the ARPES spectrum of the cuprate superconductors. In the normal state, small angle scattering from out-of-plane impurities is thought to broaden the ARPES spectral response with minimal effect on the resistivity or the superconducting transition temperature T_c. Here we explore how such forward scattering affects the ARPES spectrum in the *d*-wave superconducting state. Away from the nodal direction, the one-electron impurity scattering rate is found to be suppressed as ω approaches the gap edge by a cancellation between normal and anomalous scattering processes, leading to a square-root-like feature in the spectral weight as ω approaches $-\Delta_{\mathbf{k}}$ from below. For momenta away from the Fermi surface, our analysis suggests that a dirty optimally or overdoped system will still display a sharp but nondispersive peak which could be confused with a quasiparticle spectral feature. Only in cleaner samples should the true dispersing quasiparticle peak become visible. At the nodal point on the Fermi surface, the contribution of the anomalous scattering vanishes and the spectral weight exhibits a Lorentzian quasiparticle peak in both energy and momentum. Our analysis, including a treatment of unitary scatterers and inelastic spin fluctuation scattering, suggests explanations for the sometimes mysterious line shapes and temperature dependences of the peak structures observed in the $Bi_2Sr_2CaCu_2O_8$ system.

DOI: 10.1103/PhysRevB.70.214503 PACS number(s): 74.72.−h, 74.25.Jb, 74.20.Fg

I. INTRODUCTION

Since the earliest ARPES studies of optimally doped $Bi_2Sr_2CaCu_2O_8$ (BSCCO), spectral features near the Fermi level have been reported whose width suggested the existence of a significant elastic scattering contribution which varied along the Fermi surface, taking its smallest value along the (π,π) diagonal and largest near the $(\pi,0)$ region.[1–5] The shapes of the measured energy dispersion curves (EDCs) are quite unusual, suggesting that the one-electron self-energy is also strongly energy dependent. Abrahams and Varma[6] attempted to account for both features by assuming that the self-energy was a sum of an energy-independent part arising from small-angle (forward) scattering, and a second, momentum independent term modelled with marginal Fermi liquid theory. They noted that the elastic forward scattering was most probably associated with impurities which were located away from the CuO_2 planes and reflected the $v_F(\mathbf{k})^{-1}$ variation of the momentum-resolved density of states as $\mathbf{k}$ moved around the Fermi surface. They further remarked that, despite the large scattering rates of order 100 meV deduced from fits to ARPES spectra, the forward scattering nature of the disorder would be consistent with such scattering having a negligible effect on the resistivity of the optimally doped cuprates.[7] In addition, it was shown that this type of disorder would have a small effect on T_c.[8,9]

There are two obvious difficulties with this scenario. The first is that the spectral peak measured by ARPES near the $(\pi,0)$ point is known to sharpen dramatically when one goes below T_c, a phenomenon interpreted as the formation of a coherent quasiparticle in the superconducting state. This sharpening has normally been attributed to the well-known collapse of the inelastic scattering rate below T_c due to the opening of the superconducting gap, but it is hard *a priori* to guess why something similar should happen in the presence of an elastic scattering rate of order 100 meV. We here will argue that this difficulty need not invalidate the basic premise of Abrahams and Varma.[6] The second problem is that recently increased momentum resolution[5] and the use of different photon energies[10–13] has resolved a bilayer splitting which has its maximum effect near the $(\pi,0)$ point. Some of the previously observed "elastic broadening" is therefore certainly due to this as well as to pseudogap effects,[14] but exactly how much is not clear.

On the other hand, one cannot ignore the out-of-plane disorder. The BSCCO material is thought to be doped by excess oxygen in the SrO and BiO planes, and even the best single crystals are believed to contain significant amounts of cation switching and other out-of-plane defects.[15] It is therefore reasonable to assume that quasiparticles moving in the CuO_2 planes of this material must experience a smooth potential landscape due to these defects, and useful to pursue the question of the effect of this type of scattering in the superconducting state. In fact, fits[16] to Fourier transformed-scanning tunnelling spectroscopy measurements[17] on similar samples to those used in the ARPES studies have recently been shown to require both a strong (near-unitary limit) scattering component, attributed to native defects in the CuO_2 planes, as well as a weaker, smooth scattering potential component attributed to defects away from the plane. Recently, Markiewicz has also attempted to relate STM and ARPES data in the superconducting state assuming a smooth potential.[18]

In this work we model the complex collection of out-of-plane defects with a simple set of impurity potentials with finite range, and find a number of surprising results. The first is that the elastic scattering rate indeed "collapses" in the

superconducting state in the strong forward scattering limit, leading to a sharp spectral feature everywhere on the Fermi surface except at the nodal point itself. The second is that as one goes away from the Fermi surface, this feature disperses away as expected for a quasiparticle peak *only* if the system is sufficiently clean; otherwise it remains pinned to the gap edge. This would appear to explain the apparent lack of quasiparticle dispersion in older samples. In some situations both a nondispersive gap edge peak and a dispersing quasiparticle feature can be simultaneously observed. While we do not attempt a direct fit to experiment, we show that assuming a rather simple and physically motivated model for the one electron self-energy, which combines the above description of forward elastic scattering with strong pointlike elastic scattering and spin fluctuation inelastic scattering, allows us to calculate a spectral function which appears to reproduce many of the qualitative features of current ARPES data on optimally to overdoped cuprates. It is our hope that the ideas presented here can help unravel some of the mysteries surrounding the behavior of what is generally called the superconducting "quasiparticle peak," and allow a more accurate description of the actual propagating excitation. They will also have important immediate implications for other bulk properties of the superconducting state.

The paper is organized as follows. Section II discusses general effects of extended impurities scattering on the ARPES spectrum in both the normal and superconducting states. In Sec. III, we examine the effect of adding an isotropic elastic scattering due to unitary scatterers as well as the inelastic scattering due to spin fluctuations. Finally, Sec. IV contains our comparison with existing data, conclusions, and plans for future work.

II. ELASTIC SCATTERING

A. Normal state

We first consider a model system where scattering occurs only because of disorder. For simplicity, we will assume that the most important feature of the potential due to out-of-plane impurities experienced by electrons moving in the CuO_2 planes is its finite range κ^{-1}. We therefore model a single impurity simply as a term $V(r)=V_0 e^{-\kappa r}$, or

$$V_{\mathbf{k}\mathbf{k}'} = \frac{2\pi\kappa V_0}{((\mathbf{k}-\mathbf{k}')^2+\kappa^2)^{3/2}}, \tag{1}$$

where V_0 sets the strength of the potential and κ^{-1} is its range. Note that $\mathbf{k}$ and $\mathbf{k}'$ are only defined up to a reciprocal lattice vector. The self-energy due to many such impurities gives rise to an elastic broadening of quasiparticle states which depends upon the position of $\mathbf{k}$ in the Brillouin zone. For weak scattering, the Born approximation for the retarded self-energy associated with a random distribution of n_I impurities per unit area has the usual form in the normal state

$$\Sigma(\mathbf{k},\omega) = n_I \sum_{k'} |V_{\mathbf{k}\mathbf{k}'}|^2 G^0(\mathbf{k}',\omega), \tag{2}$$

where ω is understood to include an infinitesimal positive imaginary part, and the superscript on the single-particle

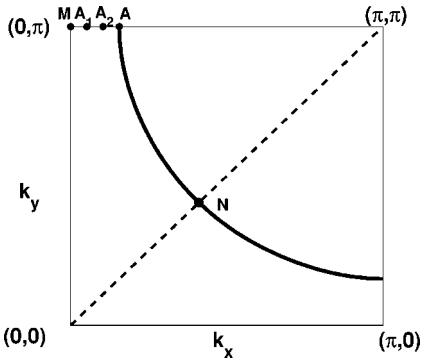

FIG. 1. The Fermi surface corresponding to the band ϵ_k given by Eq. (3) with $t'/t=-0.35$ and $\mu=-1$. The energy distribution curves of $A(\mathbf{k},\omega)$ will be discussed for $\mathbf{k}=\mathbf{k}_N$ (nodal), $\mathbf{k}=\mathbf{k}_A$ (antinodal), and various k values along the $(0,\pi)$ to $\mathbf{k}_A$ cut shown by the solid points.

Green's function $G^0 \equiv (\omega-\epsilon_{\mathbf{k}}+\mu)^{-1}$ indicates that at first we ignore self-consistency, i.e., G^0 does not depend on Σ.

To model the electronic structure we take a simple near-neighbor hopping t and next-near-neighbor hopping t', such that

$$\epsilon_{\mathbf{k}} = -2t(\cos k_x + \cos k_y) - 4t' \cos k_x \cos k_y - \mu \tag{3}$$

and set $t'/t=-0.35$ and $\mu/t=-1$. Note that with this choice of parameters there is a van Hove singularity with a peak in the total density of states at $-0.4t$. The Fermi surface for these parameters is shown in Fig. 1; it is similar but not identical to the Fermi surfaces found for both YBCO-123 and BSCCO-2212 by ARPES.

As the range of the potential κ^{-1} increases, the scattering of a quasiparticle from $\mathbf{k}$ to $\mathbf{k}'$ becomes peaked in the forward direction. As shown in Fig. 2, when $\mathbf{k}$ is close to $\mathbf{k}'$ and both are not too far from the Fermi surface, we may parametrize them as

$$\mathbf{k} = \mathbf{k}_F + k_\perp \hat{k}_\perp, \tag{4}$$

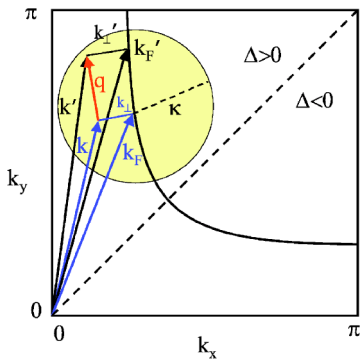

FIG. 2. (Color online) Geometry for the forward scattering process in which a quasiparticle scatters from $\mathbf{k}$ to $\mathbf{k}'$.

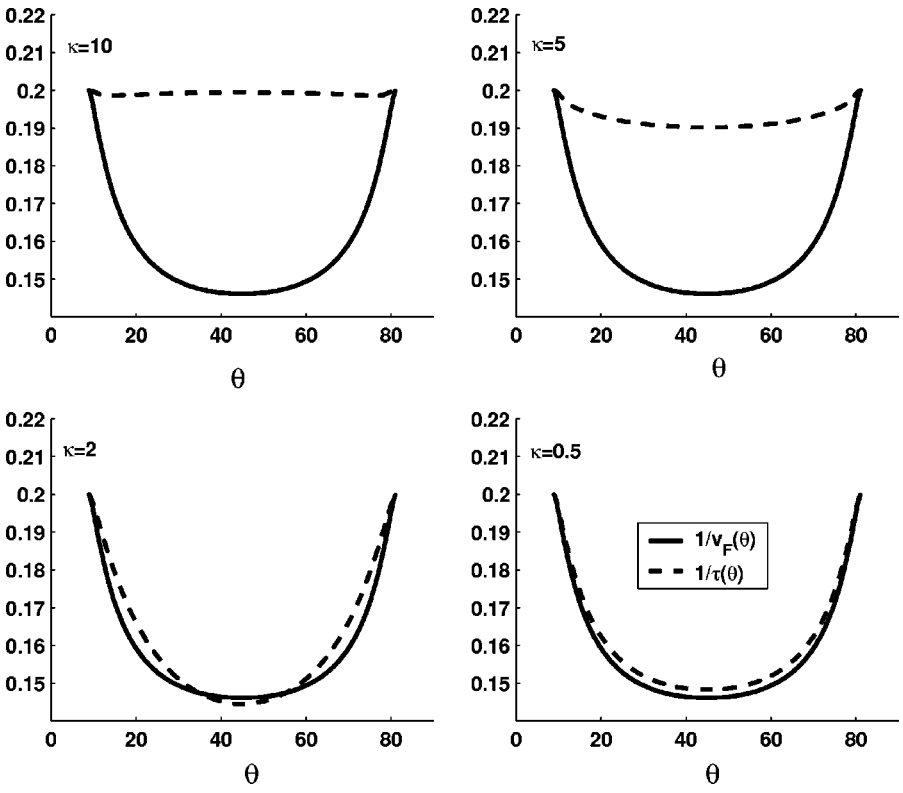

FIG. 3. The elastic scattering width $\Gamma(\mathbf{k})=-\mathrm{Im}\,\Sigma(\mathbf{k}_F,0)$ in units of t plotted around the Fermi surface with $\theta=\tan^{-1}(k_y/k_x)$. Results are shown in Figs. 2(a)–2(d) for $\kappa=10$, 5, 2, and 0.5, respectively, with $n_I|V_0|^2$ adjusted so that $\Gamma_{\max}=-\mathrm{Im}\,\Sigma(\mathbf{k}_A,0)$ is equal to $0.2t$. The dashed curve is proportional to $v_F^{-1}(\theta)$ and one sees that as κ decreases and the scattering peaks in the forward direction, $\Gamma(\mathbf{k})$ varies as $v_F^{-1}(\theta)$.

$$\mathbf{k}'=\mathbf{k}_F+\mathbf{q}_\parallel+k'_\perp\hat{k}'_\perp, \tag{5}$$

where $\mathbf{q}=\mathbf{k}-\mathbf{k}'$ is the momentum transfer and $\mathbf{q}_\parallel$ its component parallel to the Fermi surface. The unit vectors $\hat{k}_\perp$ and $\hat{k}'_\perp$ are the projections of $\mathbf{k}$ and $\mathbf{k}'$ onto the Fermi surface, respectively, such that, e.g., $\epsilon_{\mathbf{k}'}=v_F(\mathbf{k}')k'_\perp$. The imaginary part of the retarded self-energy (2) becomes

$$\Sigma''(\mathbf{k},\omega)=\frac{-n_i(2\pi\kappa V_0)^2}{(2\pi)^2}\int\frac{dk'_\parallel\,dk'_\perp}{[q^2+\kappa^2]^3}\delta(\omega-\epsilon_{\mathbf{k}'}) \tag{6}$$

$$\simeq-\frac{n_i\kappa^2V_0^2}{|v_F(k_\parallel)|}\int\frac{dq'_\parallel}{\left[q'^2_\parallel+\left(k_\perp-\frac{\omega}{v_F}\right)^2+\kappa^2\right]^3} \tag{7}$$

$$\simeq-\frac{3\pi n_iV_0^2}{8|v_F(k_\parallel)|\kappa^3}\frac{1}{\left[\left(\frac{\epsilon_k-\omega}{v_F(k_\parallel)\kappa}\right)^2+1\right]^{5/2}}. \tag{8}$$

Equation (8) shows explicitly that in the limit of small κ, the self-energy becomes more and more sharply peaked "on the mass shell" $\omega=\epsilon_k$. This is a generic feature of long-range potentials. For example, on the Fermi surface $\mathbf{k}=\mathbf{k}_F$ at $\omega=0$,

$$-\Sigma''(\mathbf{k}_F,0)\equiv\Gamma_0(\mathbf{k}_F)=\frac{3\pi n_iV_0^2}{8|v_F(\mathbf{k}_F)|\kappa^3}. \tag{9}$$

In Fig. 3, we show how this angular dependence $\propto 1/|v_{\mathbf{k}_F}|$ is approached by the exact result (2) as κ decreases and the range of the scattering is increased. In the figure and in what follows in this section, we will use the result (9) with $n_I|V_0|^2$ chosen such that $\Gamma_0(\mathbf{k}_A)=0.2t$ corresponding to $\Gamma_0(\mathbf{k}_A)\simeq 30$ meV for $t=0.15$ eV. From Fig. 3 we see that in the forward scattering limit, $\Gamma_0(\mathbf{k}_N)\simeq\Gamma_0(\mathbf{k}_A)/1.4\simeq 0.14t$. We stress that the precise dependence of the forward elastic part of the self-energy (9) on κ and on momentum depend on the details of the Fermi surface shape and impurity scattering potential. However, we do not expect qualitative features of the resulting spectra to be affected. We note further that the absolute magnitudes of the parameters chosen are roughly consistent with the $\mathcal{O}(10\%)$ weak scatterers of strength V_0 of $\mathcal{O}(t)$ and range of $\mathcal{O}(1-2a)$ extracted from FT-STS data in Ref. 16. In Sec. III, we will show results for various values of $\Gamma_0(\mathbf{k}_A)$ and κ.

Thus far we have not considered the effect of self-consistency, i.e., replacing G^0 in Eq. (2) by $G(\mathbf{k},\omega)=[(G^0)^{-1}-\Sigma]^{-1}$. In the normal metal one is used for ignoring this distinction, as the self-consistent solution for pointlike scatterers can be shown to be identical to the non-self-consistent one up to corrections of order $(\omega/E_F)^2$, where E_F is the Fermi energy. If the scatterers have a finite range, however, this argument breaks down and self-consistency becomes important. As seen in Fig. 4, the effect of self-consistency is to reduce the frequency dependence of $\Sigma''(\mathbf{k},\omega)$ induced by electronic structure; in particular, the van Hove singularity at $\omega=-0.4t$ is eliminated. This may account for the complete absence of van Hove spectral features in STM and other tunnelling experiments on BSCCO. We note further that the scattering rate is cut off in the forward scattering case $\kappa=0.5$ when $|\omega|>v_F\kappa$, reflecting the fact that if the electron's momentum can only be shifted by a small amount $\sim\kappa$, the allowed energy transfer is also restricted.

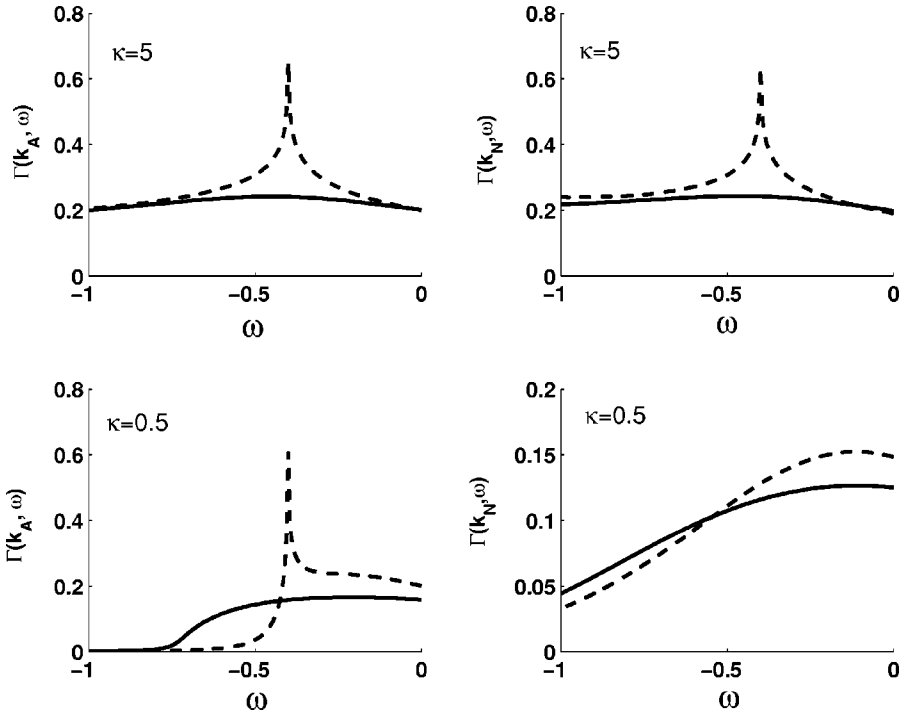

FIG. 4. Scattering rate $\Gamma(\mathbf{k},\omega) = -\mathrm{Im}\,\Sigma(\mathbf{k},\omega)$ for $\mathbf{k}$ on the Fermi surface at points A (left) and N (right), for two different values of forward scattering parameter $\kappa = 5$ (top) and 0.5 (bottom). Here, as in Fig. 3, $n_i V_0^2$ has been chosen to give $\Gamma(\mathbf{k}_A) = 0.2t$. Dashed curves, non-self-consistent Born approximation; solid curves, self-consistent Born approximation.

B. Superconducting state

1. Elastic self-energy

To describe the superconducting state, we assume a BCS d-wave order parameter corresponding to pure nearest-neighbor pairing,

$$\Delta_{\mathbf{k}} = \frac{\Delta_0}{2}(\cos k_x - \cos k_y)$$

with $\Delta_0/t = 0.2$. The full matrix Green's function in the presence of scattering in the superconducting state is

$$G(\mathbf{k},\omega) = \frac{\tilde{\omega}\tau_0 + \tilde{\epsilon}_{\mathbf{k}}\tau_3 + \tilde{\Delta}_{\mathbf{k}}\tau_1}{\tilde{\omega}^2 - \tilde{\epsilon}_{\mathbf{k}}^2 - \tilde{\Delta}_{\mathbf{k}}^2}, \tag{10}$$

where $\tilde{\omega} \equiv \omega - \Sigma_0$, $\tilde{\epsilon}_{\mathbf{k}} \equiv \epsilon_{\mathbf{k}} + \Sigma_3$, $\tilde{\Delta}_{\mathbf{k}} \equiv \Delta_{\mathbf{k}} + \Sigma_1$, and the Σ_α are the components of the self-energy proportional to the Pauli matrices τ_α in particle-hole space. If we first assume the simplest case, that the scattering is entirely elastic and weak, we may approximate the self-energy in the Born approximation similar to (2) as

$$\underline{\Sigma} = n_I \sum_{k'} |V_{\mathbf{k}\mathbf{k}'}|^2 \tau_3 \underline{G}^0(\mathbf{k}',\omega)\tau_3, \tag{11}$$

with Nambu components

$$\Sigma_0(\mathbf{k},\omega) = n_I \sum_{\mathbf{k}'} |V(\mathbf{k},\mathbf{k}')|^2 \frac{\omega}{\omega^2 - \epsilon_{\mathbf{k}'}^2 - \Delta_{\mathbf{k}'}^2}, \tag{12}$$

$$\Sigma_3(\mathbf{k},\omega) = n_I \sum_{\mathbf{k}'} |V(\mathbf{k},\mathbf{k}')|^2 \frac{\epsilon_{\mathbf{k}'}}{\omega^2 - \epsilon_{\mathbf{k}'}^2 - \Delta_{\mathbf{k}'}^2}, \tag{13}$$

and

$$\Sigma_1(\mathbf{k},\omega) = -n_I \sum_{\mathbf{k}'} |V(\mathbf{k},\mathbf{k}')|^2 \frac{\Delta_{\mathbf{k}'}}{\omega^2 - \epsilon_{\mathbf{k}'}^2 - \Delta_{\mathbf{k}'}^2}. \tag{14}$$

We will calculate the self-energies both non-self-consistently, as in Eq. (11), and self-consistently by requiring that $\underline{\Sigma}[G^0] \rightarrow \underline{\Sigma}[G]$. In Fig. 5, we show the variation of these self-energy components with energy at $\mathbf{k} = \mathbf{k}_N$ and $\mathbf{k} = \mathbf{k}_A$. Again the van Hove singularity is washed out in the self-consistent evaluation, and it is furthermore noteworthy that the Σ_3 component becomes quite small in the forward scattering limit. While in Fig. 5 gaps appear in the Σ_α near the A point for small κ, the values of Σ_0 and Σ_1 near the gap edge $\omega \gtrsim \Delta_{\mathbf{k}'}$ are large, of order several times the hopping t. Quasiparticle properties near the Fermi surface are determined, however, by particular combinations of the Nambu self-energy components. As can immediately be seen from the denominator of (10), the total elastic scattering rate broadening the quasiparticle state of energy ω will be

$$\Gamma_{\mathrm{el}}(\mathbf{k}) \simeq -\mathrm{Im}\left(\Sigma_0(\mathbf{k},\omega) + \frac{\Delta_{\mathbf{k}}}{\omega}\Sigma_1(\mathbf{k},\omega)\right), \tag{15}$$

provided one can neglect Σ_3 (see Fig. 5). In Fig. 6, we see that as ω goes to $-\Delta(\mathbf{k}_A)$ for $\mathbf{k} = \mathbf{k}_A$, Γ_{el} is suppressed by the near cancellation of the two components in (15) when κ becomes small. To obtain some insight into the physical origins of this cancellation, we derive approximate analytical forms for $\kappa \ll 1$ following the discussion of the normal state above, leading to

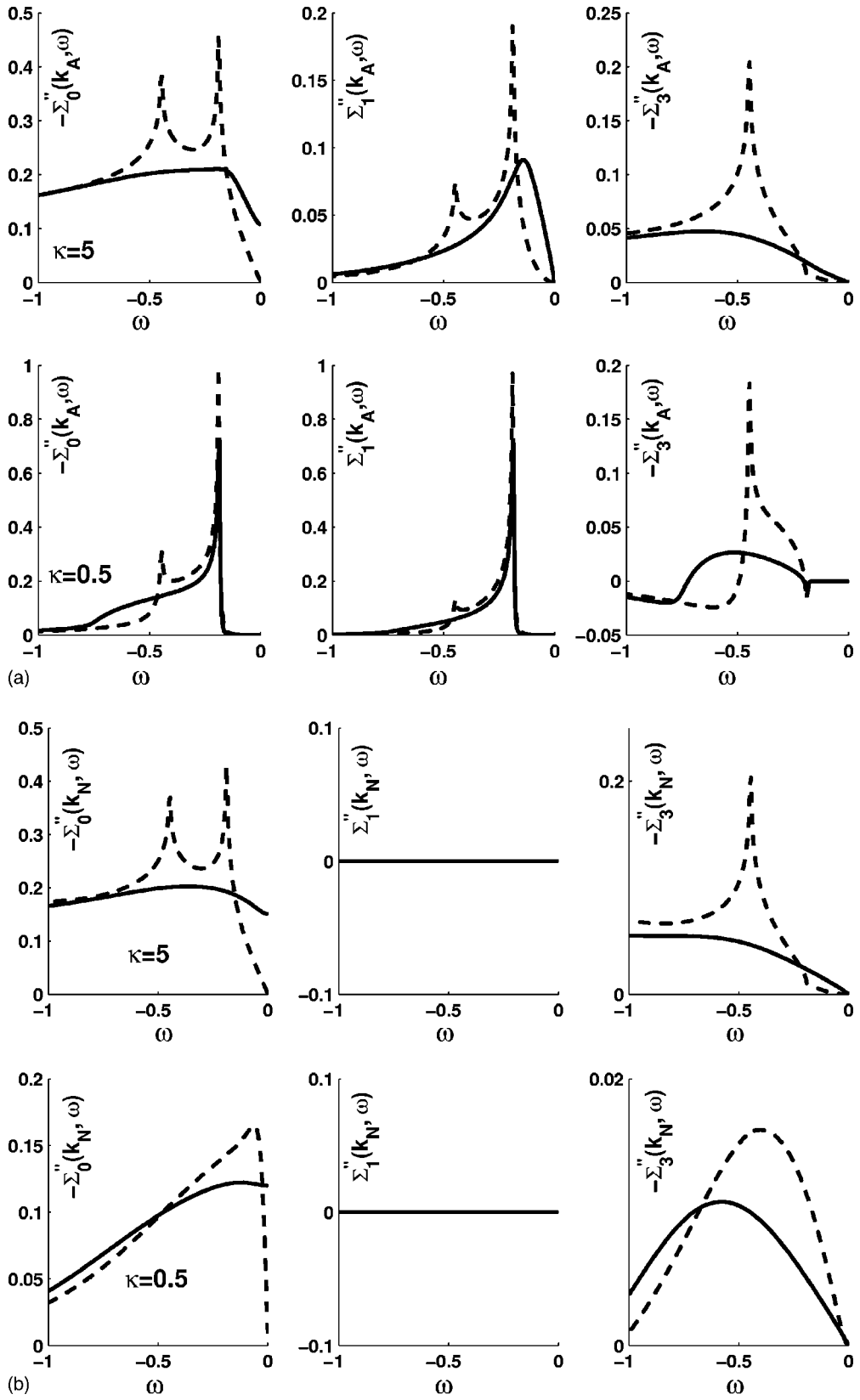

FIG. 5. The self-energy terms $-\mathrm{Im}\,\Sigma_0(\mathbf{k},\omega)$, $\mathrm{Im}\,\Sigma_1(\mathbf{k},\omega)$, and $-\mathrm{Im}\,\Sigma_3(\mathbf{k},\omega)$ in the superconducting state at $T=0$ for $\mathbf{k}=\mathbf{k}_A$ (top) and $\mathbf{k}_N$ (bottom), for $\kappa=5$ and 0.5 and the same band and scattering parameters as previously used. Here $\Delta_k=\Delta_0\,(\cos_x-\cos k_y)/2$ with $\Delta_0=0.2t$.

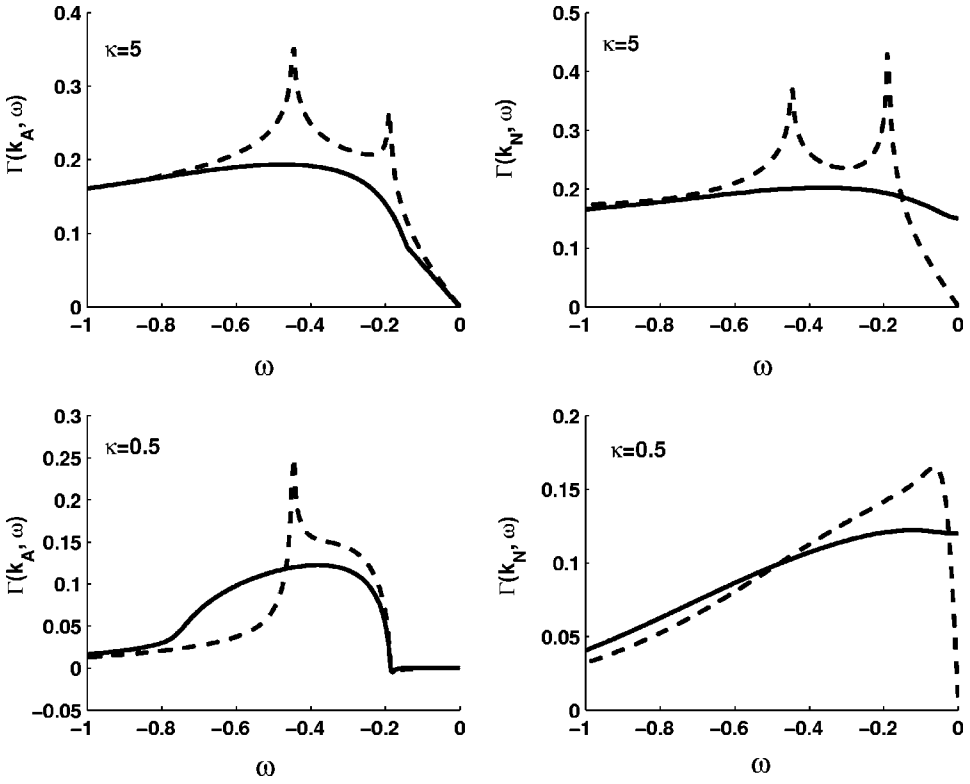

FIG. 6. Scattering rate $\Gamma_{\rm el}(\mathbf{k},\omega)$ vs ω for $\mathbf{k}=\mathbf{k}_A$ (left) and $\mathbf{k}_N$ (right) in the superconducting state at $T=0$, for $\kappa=5$ (top) and $\kappa=0.5$ (bottom). Here $\Gamma_0(\mathbf{k}_A)=0.2t$.

$$\Sigma''_\alpha(\mathbf{k},\omega) \simeq -\frac{\Gamma_0(\mathbf{k}_F)}{2\sqrt{\omega^2-\Delta_{\mathbf{k}}^2}} \sum_{\nu=\pm 1} s_\alpha \times \left[\left(\frac{\epsilon_k - \nu\sqrt{\omega^2-\Delta_{\mathbf{k}}^2}}{\kappa v_F(\mathbf{k})}\right)^2 + 1\right]^{-5/2}. \quad (16)$$

Here $s_\alpha=|\omega|$, $-\Delta_{\mathbf{k}}$ sgn ω, and ν sgn $\omega\sqrt{\omega^2-\Delta_{\mathbf{k}}^2}$ for the Nambu components $\alpha=0,1$, and 3, respectively, and $\Gamma_0(\mathbf{k})$ is given by Eq. (9). Note that Σ''_3 vanishes on the Fermi surface $\epsilon_{\mathbf{k}}=0$ in this limit. In order to gain some further intuition for these expressions, we specialize to the case where the momentum $\mathbf{k}$ is close to the Fermi surface and the energies ω are small, such that $|(\epsilon_k \pm \sqrt{\omega^2-\Delta_k^2})/\kappa v_F(\mathbf{k})| \ll 1$. The self-energies may then be written

$$\Sigma''_0(\mathbf{k},\omega) \sim -\Gamma_0(\mathbf{k}_F)\frac{|\omega|}{\sqrt{\omega^2-\Delta_{\mathbf{k}}^2}}, \quad (17)$$

$$\Sigma''_1(\mathbf{k},\omega) \sim \Gamma_0(\mathbf{k}_F)\frac{\Delta_{\mathbf{k}}\,\mathrm{sgn}\,\omega}{\sqrt{\omega^2-\Delta_{\mathbf{k}}^2}}, \quad (18)$$

$$\Sigma''_3(\mathbf{k},\omega) \simeq 0, \quad (19)$$

but are strongly supressed due to energy conservation when $|\sqrt{\omega^2-\Delta_{\mathbf{k}}^2}-\epsilon_{\mathbf{k}}|$ becomes greater than κv_F, as one may observe in Fig. 5. These equations are now identical in form to those expected for an *s*-wave superconductor (even when self-consistency is included). All peculiarities of the *d*-wave state which result from momentum averaging over the Fermi surface have disappeared. We therefore expect *a priori* to recover Anderson's theorem, the insensitivity of bulk thermodynamic properties to nonmagnetic scattering.[19] The physical reason for this is clear: as seen in Fig. 2, for small κ and $\mathbf{k}$ a distance at least κ from the node, small angle scattering cannot mix order parameters of different signs, and therefore cannot break Cooper pairs. The analogy with the *s*-wave superconductor and relation to Anderson's theorem in the context of ARPES is discussed further in the Appendix. In addition, the slowing of the rate of T_c suppression due to disorder as scattering becomes more anisotropic was treated some time ago by several authors.[8] These works were motivated by T_c suppression rates in the cuprates which appear to be 2–3 times slower than predicted by the classic Abrikosov-Gorkov formula[20] appropriate for pointlike isotropic scatterers. The suppression of T_c near the pure forward scattering limit has been discussed recently in detail by Kee.[9]

In the forward scattering limit where Eqs. (17)–(19) hold, the effective elastic scattering rate (15) becomes

$$\Gamma_{\rm el}(\mathbf{k},\omega) \simeq \Gamma_0(\mathbf{k}_F)\frac{\sqrt{\omega^2-\Delta_{\mathbf{k}}^2}}{|\omega|}, \quad |\omega| \gtrsim |\Delta_{\mathbf{k}}|. \quad (20)$$

For $\mathbf{k}$ along the nodal direction, the elastic broadening in the superconducting *d*-wave state is equal to its value in the normal state. However, for $\mathbf{k}$ in the antinodal region, the broadening vanishes as $\omega \to \Delta_{\mathbf{k}}$ and approaches the normal state value only when ω becomes large compared with $\Delta_{\mathbf{k}}$. The elastic contribution $\Gamma_{\rm el}(\mathbf{k}_A,\omega)$ to the broadening at the antinodal $\mathbf{k}_A$ point versus ω is shown in Fig. 6. Physically, the individual contributions to the normal $\Sigma_0(\mathbf{k},\omega)$ and anomalous $\Sigma_1(\mathbf{k},\omega)$ self-energies are both enhanced by the density of states factor $(\omega^2-\Delta^2(\mathbf{k}))^{-1/2}$ (Fig. 5). However, the normal contribution describing the scattering out of state $\mathbf{k}$ into $\mathbf{k}'$ is compensated by the anomalous contribution scat-

tering into $\mathbf{k}$ from the pair condensate. This gives rise to the suppression of the elastic scattering seen in Fig. 6 relative to Fig. 5 as ω approaches $-|\Delta_{\mathbf{k}_A}|$ from below.

2. Spectral function

The near-cancellation of the two Nambu components of the self-energy near the gap edge in the forward scattering limit leads to a dramatically reduced *elastic* scattering rate in the superconducting state, which sharpens the spectral features of quasiparticles which are not too close to the nodes. Within the current model where we continue to neglect inelastic scattering due to electron-electron interactions, we now turn to the one-electron spectral function measured by ARPES. In the forward scattering limit, with the self-energy given by Eqs. (17)–(19), one obtains a result for the Green's function previously discussed by Markiewicz,[18]

$$\underline{G}(\mathbf{k},\omega) \simeq \frac{(\omega\tau_0 + \Delta_{\mathbf{k}}\tau_1)z(\mathbf{k},\omega) + \epsilon_k\tau_3}{(\omega^2 - \Delta_{\mathbf{k}}^2)z(\mathbf{k},\omega)^2 - \epsilon_k^2}. \tag{21}$$

Here $z(\mathbf{k},\omega)=1+i\Gamma_0(\mathbf{k})\mathrm{sgn}\,\omega/\sqrt{\omega^2-\Delta_k^2}$. The electron component of the spectral function is then

$$A(\mathbf{k},\omega) = -\frac{1}{\pi}\,\mathrm{Im}\,G_{11}(\mathbf{k},\omega) = -\frac{1}{\pi}\,\mathrm{Im}\,\frac{\omega z(\mathbf{k},\omega) + \epsilon_{\mathbf{k}}}{(\omega^2 - \Delta_{\mathbf{k}}^2)z(\mathbf{k},\omega)^2 - \epsilon_k^2}. \tag{22}$$

It is useful to consider a few special cases of (22) more closely. In particular, on the Fermi surface $\epsilon_{\mathbf{k}}=0$ one has the simple expression

$$A(\mathbf{k}_F,\omega) = \frac{\Gamma_0(\mathbf{k})}{\pi}\frac{1}{\sqrt{\omega^2-\Delta_{\mathbf{k}}^2}}\frac{|\omega|}{\omega^2 - \Delta_{\mathbf{k}}^2 + \Gamma_0(\mathbf{k})^2}, \tag{23}$$

while near the gap edge, e.g., $\omega \lesssim -|\Delta_{\mathbf{k}}|$,

$$A(\mathbf{k},\omega) \simeq \frac{1}{\pi}\frac{\Gamma_0(\mathbf{k})}{\epsilon_k^2 + \Gamma_0^2(\mathbf{k})}\frac{|\omega|}{\sqrt{\omega^2-\Delta_{\mathbf{k}}^2}}. \tag{24}$$

At the nodal point $\mathbf{k}_N$, where the gap vanishes, the spectral weight is given by the simple Lorentzian form

$$A(\mathbf{k}_N,\omega) = \frac{\Gamma_0(\mathbf{k}_N)/\pi}{\omega^2 + \Gamma_0(\mathbf{k}_N)^2}, \tag{25}$$

and at low temperatures where the elastic scattering is dominant one can determine $\Gamma_0(\mathbf{k}_N)$. However, for $\mathbf{k}$ at the antinodal point $\mathbf{k}_A$ such that $-\Delta_{\mathbf{k}_A}-\delta\omega<\omega<-\Delta_{\mathbf{k}_A}$,

$$A(\mathbf{k}_A,\omega) \cong \frac{1}{\pi}\frac{\Delta_{\mathbf{k}_A}}{\Gamma_0(\mathbf{k}_A)}\frac{1}{\sqrt{\omega^2-\Delta_{\mathbf{k}_A}^2}}, \tag{26}$$

where the "width" $\delta\omega$ depends upon the ratio $\Delta_{\mathbf{k}_A}/\Gamma_0(\mathbf{k}_A)$. If $\Delta_{\mathbf{k}_A}$ is large compared with $\Gamma_0(\mathbf{k}_A)$, the width $\delta\omega \simeq \Gamma_0(\mathbf{k}_A)^2/(2\Delta_{\mathbf{k}_A})$. If one integrates $A(\mathbf{k}_A,\omega)$ from $-\Delta_{\mathbf{k}_A}-\delta\omega$ to $-\Delta_{\mathbf{k}_A}$ to define a "peak intensity"

$$I(\mathbf{k}_A) = \int_{-\Delta_{\mathbf{k}_A}-\delta\omega}^{-\Delta_{\mathbf{k}_A}} A(\mathbf{k}_A,\omega)d\omega \simeq \frac{1}{\pi}, \tag{27}$$

which is independent of $\Delta_{\mathbf{k}_A}/\Gamma_0(\mathbf{k}_A)$. However, when the system is sufficiently dirty such that $\Delta_{\mathbf{k}_A}<\Gamma_0(\mathbf{k}_A)$, the falloff of $A(\mathbf{k}_A,\omega)$ as ω decreases below $-\Delta_{\mathbf{k}_A}$ varies as $(\omega^2 - \Delta_{\mathbf{k}_A}^2)^{-1/2}$. In this case, the scale is set by $\Delta_{\mathbf{k}_A}$ and if one takes $\delta\omega=\Delta_{\mathbf{k}_A}$, the peak intensity varies as $I(\mathbf{k}_A) \sim \Delta_{\mathbf{k}_A}/\Gamma_0(\mathbf{k}_A)$. This is quite different from the usual BCS quasiparticle result which is proportional to the quasiparticle renormalization factor $z(\mathbf{k}_A)$ times a coherence factor which is $1/2$ on the Fermi surface. It should be possible to test the foward scattering scenerio by comparing the variation of $I(\mathbf{k}_A)$ with $\Delta_{\mathbf{k}_A}/\Gamma_0(\mathbf{k}_A)$.

Numerical results for the normal and superconducting spectral weights for $\omega<0$ using the self-consistent version of the self-energy (12)–(14) with $\omega\to\tilde{\omega}$, etc., for the model impurity potential (1) are shown in Fig. 7 for $\kappa=5$ and 0.5. For $\kappa=0.5$, the scattering is predominantly forward and in the superconducting state at $T=0$, the spectral weight for $\mathbf{k}_A$ is seen to sharpen at $-\Delta_{\mathbf{k}_A}$ despite the fact that the normal state broadening $\Gamma(\mathbf{k}_A)$ is in the order of the peak position. For $\mathbf{k}=\mathbf{k}_N$, the nodal spectral weight has the expected Lorentzian form with a width set by $\Gamma(\mathbf{k}_N)$. For $\kappa=5$, corresponding to a more isotropic scattering, the spectral weight for $\mathbf{k}=\mathbf{k}_A$ broadens. In the limit of isotropic impurity scattering, the $\underline{\Sigma}_1$ component of the impurity self-energy vanishes and $A(\mathbf{k}_A,\omega)$ has a Lorentzian-type broadened peak.

III. ISOTROPIC ELASTIC AND INELASTIC ELECTRON-ELECTRON SCATTERING

In addition to the forward scattering by out-of-plane impurities, in this section we consider unitary limit isotropic elastic scatterers as well as inelastic electron-electron collisions. In fact, it is the momentum and frequency dependence of the latter interaction about which one hopes to learn more from the ARPES spectrum. Here we proceed phenomenologically by writing

$$\underline{\Sigma}_{\mathrm{tot}} = \underline{\Sigma}_{\mathrm{el},f} + \underline{\Sigma}_{\mathrm{el},u} + \underline{\Sigma}_{\mathrm{inel}}. \tag{28}$$

The first term is the contribution from elastic (quasi)forward scatterers we have discussed in Sec. II. The second term represents the effect of unitary scatterers (possibly Cu vacancies) with concentration roughly $n_u \sim 0.2\%$ observed as zero-bias resonances in STM experiments. It will be treated as usual in the self-consistent T-matrix approximation,

$$\underline{\Sigma}_{\mathrm{el},u} = -\frac{n_u}{\sum_{\mathbf{k}} G(\mathbf{k},\omega)}\tau_0. \tag{29}$$

In the normal state we find a scattering rate of $\Gamma_u \simeq 10^{-3}t$, leading to an impurity bandwidth $\gamma_u \sim \sqrt{\Gamma_u\Delta_0} \sim 10^{-2}t$ (of order 1 to 2 meV). We note that the *width* of the resonance observed in STM is in fact roughly 3 times this number, consistent with the self-consistent T-matrix calculation,[21] impurity resonances are visible up to about 10 meV in experi-

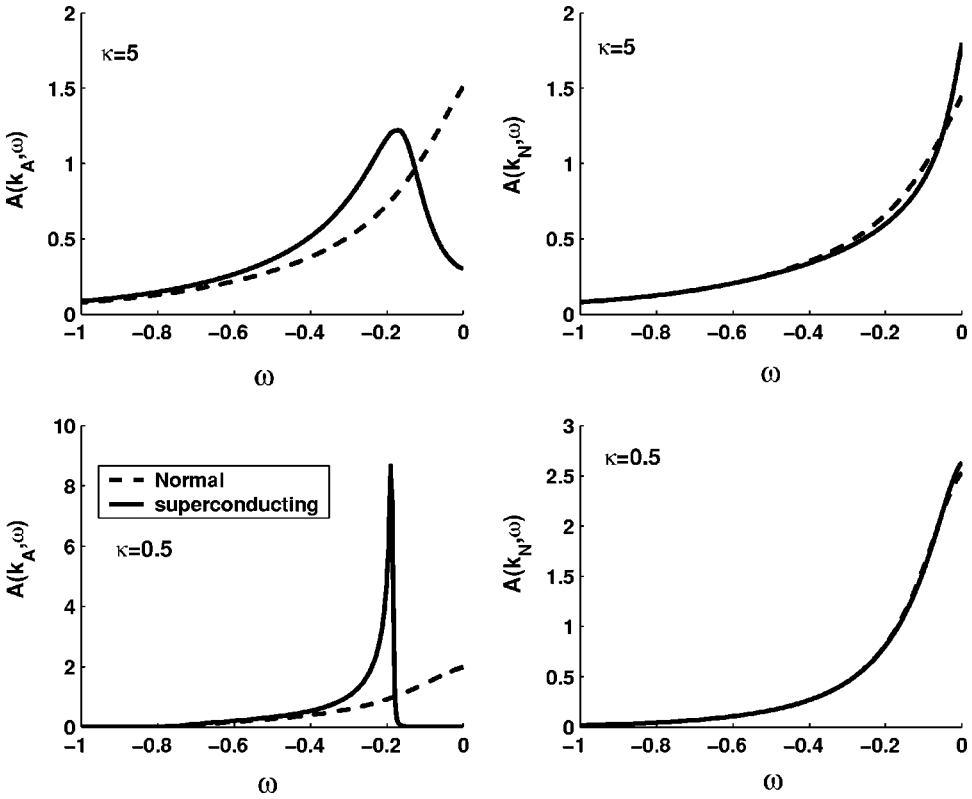

FIG. 7. Comparison of the $T=0$ self-consistent normal state (dashed) and superconducting (solid) one-electron spectral functions for $\kappa=5$ (top) and 0.5 (bottom) at $\mathbf{k}=\mathbf{k}_A$ (left) and $\mathbf{k}_N$ (right), with $\Gamma_0(\mathbf{k}_A)=0.2t$.

ments. Nevertheless the isotropic part of the elastic scattering appears to have a relatively insignificant effect on the ARPES spectral function, as shown below.

For the imaginary parts of the inelastic self-energies, we will use numerical results obtained from a spin-fluctuation calculation of the quasiparticle scattering. Following the argument leading to Eq. (15), we define an effective *inelastic* scattering rate

$$\Gamma_{\text{inel}}(\mathbf{k},\omega) = -\,\text{Im}\left(\Sigma_0^{\text{inel}}(\mathbf{k},\omega) + \frac{\Delta_{\mathbf{k}}}{\omega}\Sigma_1^{\text{inel}}(\mathbf{k},\omega)\right). \quad (30)$$

In spin-fluctuation calculations of $\Gamma_{\text{inel}}(\mathbf{k},\omega)$, it was found[22,23] that at the nodal point, at low temperatures, the scattering rate initially increased as the third power of ω or T depending upon which is larger. At other $\mathbf{k}$ points on the Fermi surface, the scattering rate varies approximately as the third power of this energy measured relative to $\Delta_{\mathbf{k}}$. The reduction of the inelastic scattering rate at low excitation energies reflects the suppression of the low energy spin fluctuations due to the opening of the *d*-wave gap. Here, we will use a numerical interpolation of the ω- and T-dependent Γ_{inel} obtained from Ref. 24.

A. The antinodal spectrum

The various contributions to the self-energy are sketched in the schematic diagram shown in Fig. 8. We will use the parameters discussed above to set the magnitudes of Σ_{inel} and $\Sigma_{\text{el},u}$. Then we will consider various values of κ and $\Gamma_0(\mathbf{k}_A)$, characterizing the forward elastic scattering. While the effect of Σ_{inel} is already contained in the intrinsic T_c and the suppression of T_c due to $\Sigma_{\text{el},u}$ is negligible for the parameters considered, this is not necessarily the case for the forward elastic scattering. As discussed by Kee,[9] the suppression of T_c varies as κ^3, so that for small values of κ such as $\kappa=0.5$,

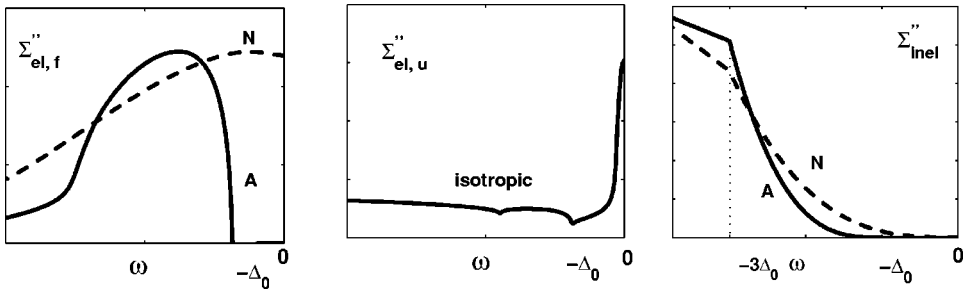

FIG. 8. Schematic depiction of the various contributions to the scattering rate in the superconducting state at $T=0$. First panel, elastic forward scattering for $\mathbf{k}=\mathbf{k}_A$ and $\mathbf{k}_N$; second panel, isotropic unitarity limit impurity scattering due to ~0.2% impurities; third panel, spin fluctuation inelastic scattering rate interpolated from Ref. 24.

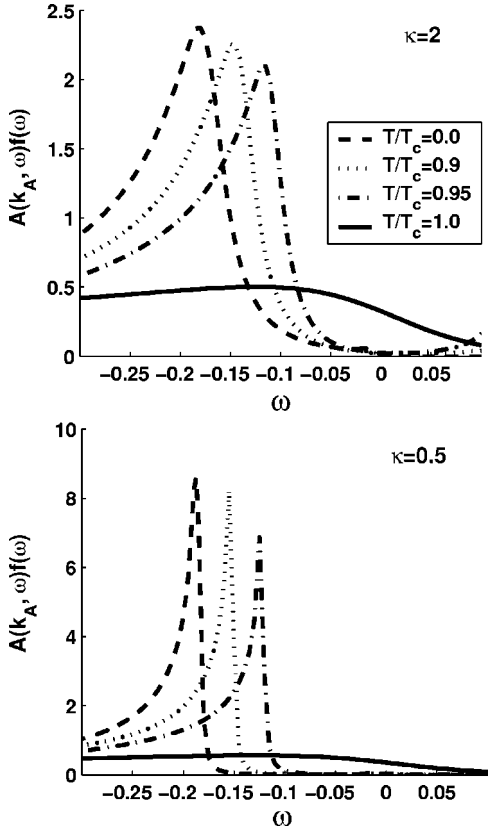

FIG. 9. Finite temperature spectral function at the antinodal point A on the Fermi surface multiplied by the Fermi function, $A(\mathbf{k}_A,\omega)f(\omega)$ vs ω including the full model self-energy as described in Sec. III. Results for $\kappa=2$ and 0.5 with $\Gamma_0(\mathbf{k}_A)=0.2t$ are shown.

the suppression of T_c is negligible for the scattering rates $\Gamma_0(\mathbf{k}_A)$ which we will consider. However, at larger values of κ this is not the case, so that the T_c shift or the lack of shift implies constraints on κ and Γ_0. For the moment, however, we will ignore this and simply compare $\kappa=0.5$ with $\kappa=2$ for three different scattering rates $\Gamma_0(\mathbf{k}_A)=0.2$, 0.1, and 0.05 in units of t corresponding to $\Gamma_0(\mathbf{k}_A)/\Delta_0=1$, 0.5, and 0.025.

In Fig. 9 we show the temperature dependence of the energy distribution curves $A(\mathbf{k},\omega)f(\omega)$ for $\mathbf{k}$ at the antinodal point $\mathbf{k}_A$. Here $f(\omega)$ is the Fermi function. In the superconducting state there is a square-root-like behavior as ω approaches $-|\Delta_{\mathbf{k}_A}|$ from below. This should be contrasted with the broad Lorentzian peak in the normal state which is cut off by $f(\omega)$. While one could understand that inelastic broadening would diminish as the temperature is lowered, the asymmetric, one-sided, square-root-like sharpening of the spectrum in the superconducting state is a consequence of forward elastic scattering as discussed in Sec. II. The peak intensity at $\mathbf{k}_A$ should scale as $\Delta_0(T)$.

B. Quasiparticle dispersion near the antinodal point

In a clean superconductor, there is a peak in the spectral function $A(\mathbf{k},\omega)$ at the quasiparticle pole $\omega=E_{\mathbf{k}}\equiv\sqrt{\epsilon_{\mathbf{k}}^2+\Delta_{\mathbf{k}}^2}$. In particular, as the momentum moves along the cut from $(\mathbf{k}_A,\pi)$ to $(0,\pi)$ shown in Fig. 1, one expects to see a dispersion of this peak to higher energies. However, if the forward elastic scattering strength $\Gamma_0(\mathbf{k}_A)\gtrsim\Delta_{\mathbf{k}_A}$, then the peak in $A(\mathbf{k},\omega)$ remains at $-\Delta_{\mathbf{k}}$ rather than dispersing. Figure 10 shows plots of $A(\mathbf{k},\omega)$ for different values of $\mathbf{k}$ between the M and A points for $\kappa=2$ and 0.5, and several values of the scattering rate $\Gamma_0(\mathbf{k}_A)$.

As samples improve, there is a natural tendency in this model for the spectrum for $\mathbf{k}$ not too far from the antinode to cross over from one characterized by a nondispersive peak at $\Delta_{\mathbf{k}}$ in the dirty limit where $\Gamma_0\sim\Delta_0$ to one characterized by a dispersive quasiparticle peak at $E_{\mathbf{k}}$ when Γ_0 is small compared to Δ_0. This crossover is due to the way in which the forward elastic scattering rate for a d-wave superconductor is reduced as the gap edge is approached and is analogous to the same effect discussed analytically in the Appendix for an s-wave superconductor. In a system with $\Gamma_0\gtrsim\Delta_0$, no quasiparticle peak is observed, but a sharp feature *does* appear at $-\Delta_{\mathbf{k}}$, representing simply the spectral weight in the overdamped quasiparticle peak piling up at the gap edge as in the s-wave case. Only when Γ_0 becomes small compared to Δ_0 does one see a true quasiparticle peak dispersing as $-E_k$. In the most strongly forward scattering case, $\kappa=0.5$, one can see that, depending on the strength of the scattering rate, one can have simultaneously a broadened dispersing feature as well as a gap edge feature. It is tempting to speculate that this phenomenon is related to the peak-dip-hump features observed generically below T_c in cuprate ARPES experiments, but we have not yet explored this issue in detail.

C. The nodal spectrum

In Fig. 11, the corresponding EDC's for the nodal k_N point are shown. In this case, the $T=0$ spectral function is a Lorentzian centered at the Fermi level, whose width is limited essentially by the elastic scattering. For the band structure parameters we have chosen, $\Gamma_0(\mathbf{k}_N)\cong\Gamma_0(\mathbf{k}_A)/1.4$, so that $\Gamma_0(\mathbf{k}_N)=0.14t$. Results in Fig. 11 are shown for several different values of $\Gamma_0(\mathbf{k}_N)$. At finite temperatures the peak is further broadened by inelastic processes. Defining a width of the asymmetric EDC's is quite difficult, a natural result of the strongly ω-dependent self-energy in the current approximation. In fact, even the shape of the EDC curve is difficult to compare directly to experiment, since it can be qualitatively changed by a small amount of averaging along the Fermi surface due to the angular resolution of the detector. If one goes a short angular distance away from the node along the Fermi surface, one finds at low T not a smooth Lorentzian for $\omega<0$, but rather a square root singularity with a small local gap $\Delta_{\mathbf{k}}$. Averaging over a small k region will therefore make the "leading edge" of this spectrum appear much sharper.

The intrinsic T-dependent broadening is therefore most clearly seen in the momentum distribution curves (MDC's), which in this work [see Eq. (25)] are simply Lorentzians centered at the Fermi surface. In Fig. 12, we show that, within this model, the rate of sharpening of the nodal MDC's indeed increases somewhat in the superconducting state as the temperature is lowered, but that the widths saturate at a value determined by the elastic scattering. The temperature

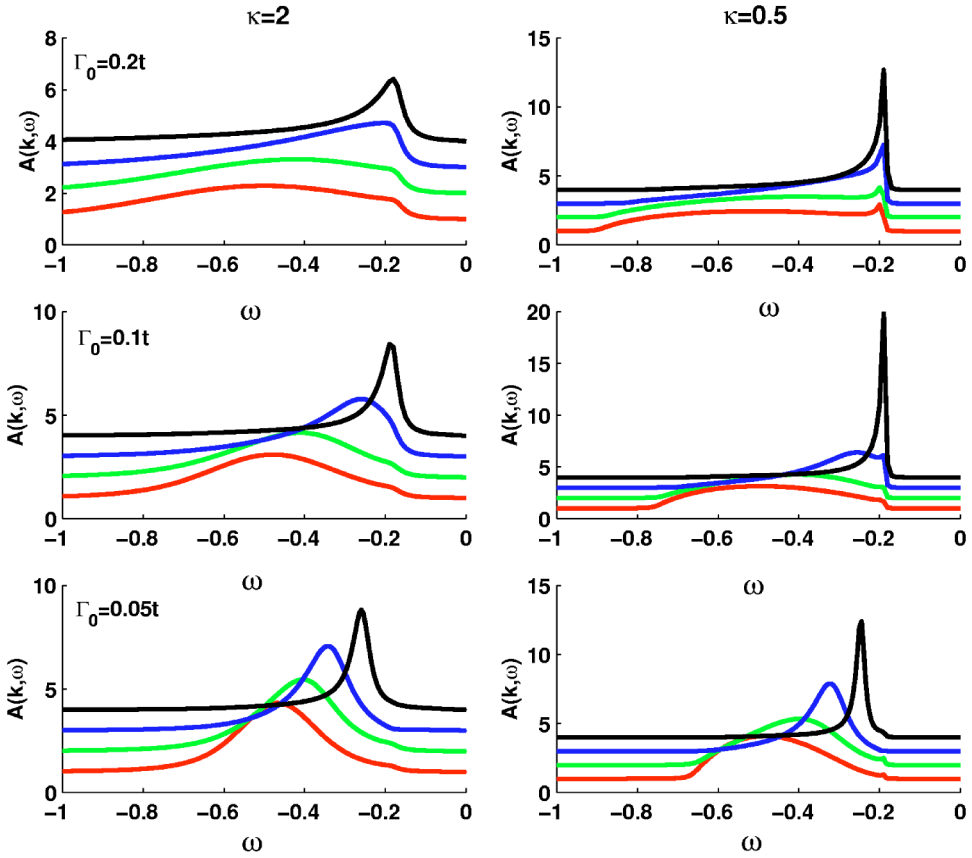

FIG. 10. $A(\mathbf{k},\omega)$ vs ω for $\kappa=2$ and 0.5. Results are given for the k points as indicated along the $(0,\pi)$, A cut in Fig. 1. The disorder levels correspond to $\Gamma_0(\mathbf{k}_A)/\Delta_0=1$, 0.5, and 0.025. Note the spectra for different $\mathbf{k}$ points have been offset for clarity.

dependence of Δk shown in Fig. 12 is in disagreement with the results of Valla *et al.*,[3] who reported a linear MDC width dependence on temperature even in the superconducting state. However, the type of ω and T dependence we find would appear to be consistent with nodal EDC linewidth measurements of Kaminski *et al.*[4]

IV. CONCLUSIONS

The main point of this work is to raise the possibility that some of the ARPES observations on optimally or overdoped samples which appeared to be in conflict with the BCS results may in fact fit within the BCS framework when the effects of forward elastic scattering are taken into account. Thus, while forward elastic scattering can be responsible for some of the anomalous width of the spectral function measured above T_c, this need not be in conflict with the observation of a sharp spectral feature in the antinodal region below T_c. Furthermore, if $\Gamma_0(\mathbf{k}_A)$ is larger than $\Delta(\mathbf{k}_A)$, the intensity associated with the area under this feature varies as $\Delta(\mathbf{k}_A)/\Gamma(\mathbf{k}_A)$, which depends upon the doping and temperature. At the same time, the spectrum at the nodal point can exhibit a Lorentzian behavior with a width that evolves smoothly through T_c and then partially narrows as the inelastic scattering is suppressed by the opening of the gap. We have seen that these effects occur because of a phenomenon similar to Anderson's theorem which applies for much of the Fermi surface of a d-wave superconductor in the forward scattering limit: if scattering is sufficiently peaked in the forward direction, the scattering process does not mix states with different signs of the order parameter, and no pair breaking occurs. Sufficiently near the nodal point, however, the sign change always takes place, implying that the full width of the quasiparticle due to elastic scattering is recovered at the nodal $\mathbf{k}_N$.

We have discussed simple approximate forms as well as fully self-consistent numerical calculations for the elastic self-energies. In the overall model for the self-energy, we also included an approximate treatment of electron-electron collisions, as well as unitary "native defect" scatterers observed to be present in the BSCCO-2212 material in STM experiments. The energy distribution curves found in the self-consistent calculations using this model show no influence of the van Hove singularity, and display an asymmetric shape with a rounded square root peak near the local gap edge. Widths and temperature dependences can be obtained which appear comparable to experiment, but it is difficult to compare directly because of the unknown ARPES background signal and bilayer splitting, which was not included here. We also discussed the temperature dependence of the momentum distribution curves in the superconducting state at the nodal point. It was found to have a Lorentzian shape which narrows with decreasing temperature in the superconducting state, due to the suppression of inelastic scattering, saturating at a value determined by the elastic scattering.

Along the momentum cut $(\mathbf{k}_A,\pi)$ to $(0,\pi)$, if $\Gamma_0(\mathbf{k}_A)$ is small compared to $\Delta_{\mathbf{k}}$, we find a dispersing quasiparticle peak at $\omega=-E_k$. However, when $\Gamma_0(\mathbf{k}_A)$ is comparable with $\Delta_{\mathbf{k}}$, the maximum response occurs for $\omega\simeq-\Delta_{\mathbf{k}}$, does not disperse as $\mathbf{k}$ moves away from the Fermi level, and can still

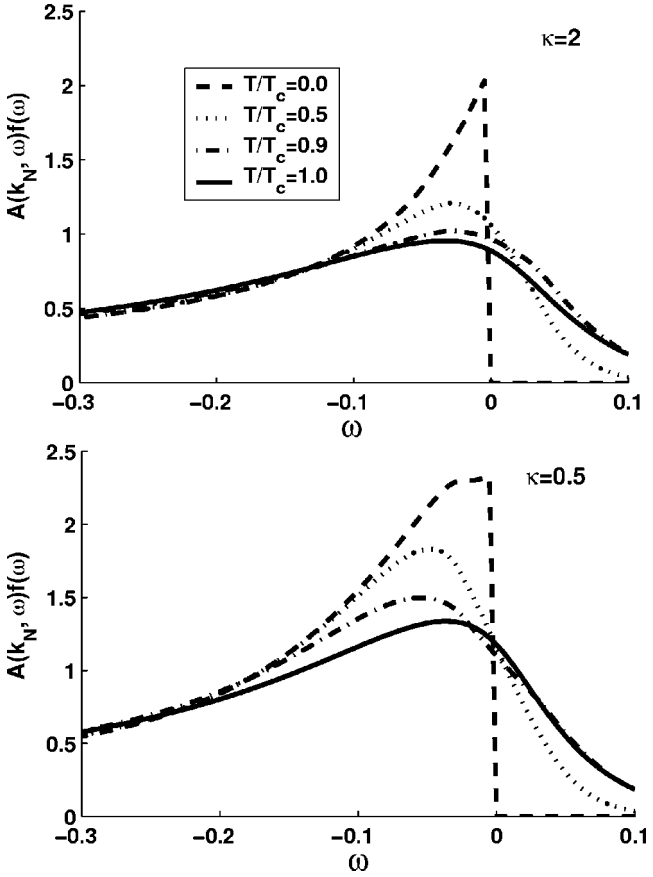

FIG. 11. (Color online) Finite temperature spectral functions at the nodal point N on the Fermi surface, $A(\mathbf{k}_N,\omega)f(\omega)$ vs ω including the full model self-energy as described in Sec. III for $\kappa=2$ and 0.5, with $\Gamma_0(\mathbf{k}_N)=0.14t$.

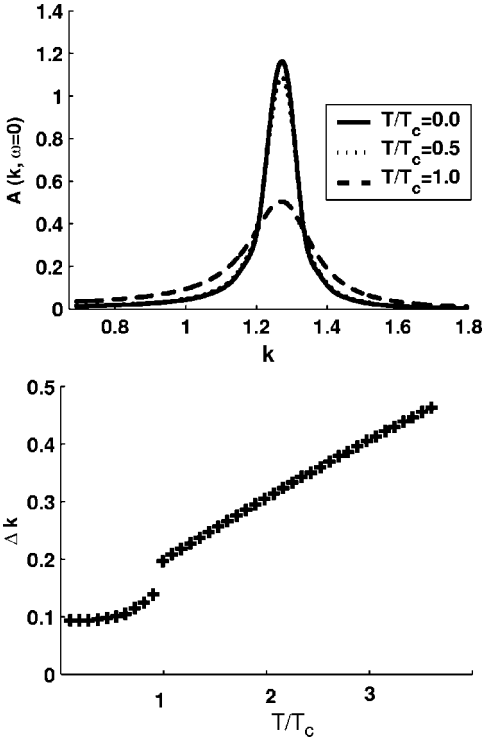

FIG. 12. (a) Finite temperature spectral function near the nodal point N along a cut perpendicular to the Fermi surface at N, $A(\mathbf{k},\omega=0)$ vs $\mathbf{k}$, including full model self-energy with $\kappa=0.5$ and $\Gamma_0(\mathbf{k}_N)=0.14t$. (b) The half-width of $A(\mathbf{k},\omega=0)$ at half-maximum, Δk, plotted vs T/T_c.

represent a sharp spectral feature. This is similar to some of the older data on the BSCCO-2212 system, which has not been explained in this paper and might have been taken for some new type of dispersionless excitation in the superconducting state. However, as we have shown, it is simply the consequence of forward elastic scattering which is suppressed at the gap edge in the superconducting state.

Here we have focussed primarily on the effects of forward elastic scattering on the BSCCO-2212 ARPES spectrum, and found that a model of several percent weak out-of-plane scatterers with a range of order one lattice spacing, similar to current models of Fourier transform STM measurements, can explain many qualitative features of the ARPES data. We believe that the unique way in which this material is doped and disordered using current crystal growth techniques endows it with an effective disorder potential which strongly influences the low-energy quasiparticle properties in a way which is characteristically different from the much cleaner YBCO system, for example. This picture should have important and calculable consequences for other superconducting properties, such as microwave conductivity, which we explore elsewhere.

ACKNOWLEDGMENTS

The authors thank E. Abrahams, N. Ingle, D. Maslov, M. R. Norman, and Z. X. Shen for enlightening discussions. Partial support was provided by ONR N00014-04-0060 and NSF DMR02-11166.

APPENDIX: ONE-ELECTRON SPECTRAL FUNCTION IN A DISORDERED *s*-WAVE SUPERCONDUCTOR

Insight into the spectral function of a *d*-wave superconductor with $\mathbf{k}$ near the antinodal point and reasonably forward scattering can be gained by examining the spectral function of an *s*-wave superconductor with disorder. Although quite simple, we are not aware that the spectral weight for an *s*-wave superconductor with isotropic impurity scattering has been discussed elsewhere. For simplicity, we restrict our consideration to isotropic, weak, nonmagnetic scatterers. The self-energies in the Born limit for a system with particle-hole symmetry and an isotropic order parameter Δ are

$$\Sigma_0 = n_i V^2 \sum_{\mathbf{k}} \frac{\tilde{\omega}}{\tilde{\omega}^2 - \epsilon_{\mathbf{k}}^2 - \tilde{\Delta}^2} = -i\Gamma \frac{u \,\mathrm{sgn}\, u'}{\sqrt{u^2-1}}, \tag{A1}$$

$$\Sigma_1 = n_i V^2 \sum_{\mathbf{k}} \frac{\tilde{\Delta}}{\tilde{\omega}^2 - \epsilon_{\mathbf{k}}^2 - \tilde{\Delta}^2} = i\Gamma \frac{\mathrm{sgn}\, u'}{\sqrt{u^2-1}}, \tag{A2}$$

$$\Sigma_3 = 0, \tag{A3}$$

where $u=\tilde{\omega}/\tilde{\Delta}$ and u' is Re u. The self-consistency equation is then

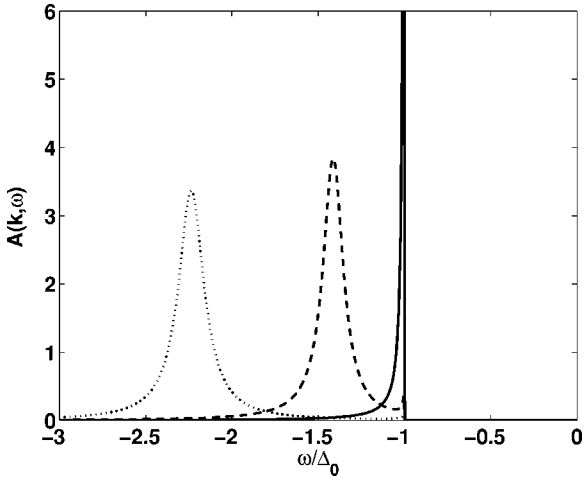

FIG. 13. $A(\mathbf{k},\omega)$ for an s-wave superconductor vs ω/Δ for $\Gamma/\Delta=0.1$ for three values (solid, dashed, dotted) of $\epsilon_{\mathbf{k}}/\Delta=0$, -1, -2.

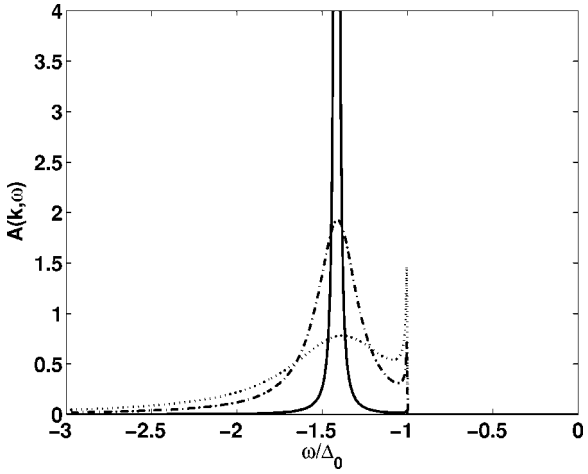

FIG. 14. $A(\mathbf{k},\omega)$ for an s-wave superconductor vs ω/Δ for $\varepsilon_{\mathbf{k}}/\Delta=-1$ for three values (solid, dashed, dotted) of $\Gamma/\Delta=0.01$, 0.2, 0.5.

$$u=\frac{\omega-\Sigma_0}{\Delta+\Sigma_1}=\frac{(\omega/\Delta)\sqrt{u^2-1}+i\,\mathrm{sgn}\,u'\overline{\Gamma}u}{\sqrt{u^2-1}+i\,\mathrm{sgn}\,u'\overline{\Gamma}}, \tag{A4}$$

with $\overline{\Gamma}=\Gamma/\Delta$, which has the solution

$$u=\frac{\tilde{\omega}}{\tilde{\Delta}}=\frac{\omega}{\Delta}. \tag{A5}$$

This means, as is well known, that the density of states

$$\rho(\omega)=\mathrm{Re}\,\frac{\tilde{\omega}\,\mathrm{sgn}\,\omega}{\sqrt{\tilde{\omega}^2-\Delta^2}}=\frac{|\omega|}{\sqrt{\omega^2-\Delta^2}}, \tag{A6}$$

is not changed by this type of impurity scattering and there is no renormalization of the momentum-integrated thermodynamic properties. This is the essence of "Anderson's theorem."[19] On the other hand, one might expect that the spectral weight $A(\mathbf{k},\omega)$ for a quasiparticle of momentum $\mathbf{k}$ should be broadened by disorder since the scattering mixes different momentum states. This is the case in the normal state where the spectral weight in the presence of impurity scattering becomes a Lorentzian of width 2Γ. To determine what happens in the superconducting state we need the 11 component of the Nambu Green's function

$$G_{11}(\mathbf{k},\omega)=\frac{\left(1+\dfrac{i\Gamma\,\mathrm{sgn}\,\omega}{\sqrt{\omega^2-\Delta^2}}\right)\omega+\epsilon_k}{\left(1+\dfrac{i\Gamma\,\mathrm{sgn}\,\omega}{\sqrt{\omega^2-\Delta^2}}\right)^2(\omega^2-\Delta^2)-\epsilon_k^2}. \tag{A7}$$

In Fig. 13, we plot the spectral function $A(\mathbf{k},\omega)=-\mathrm{Im}\,G_{11}(\mathbf{k},\omega)/\pi$ for $\omega<0$ for various values if k on and near the fermi surface. Since $i\Gamma/\sqrt{\omega^2-\Delta^2}$ is pure real for $|\omega|/\Delta<1$, the spectral weight vanishes for energies $|\omega|<\Delta$ the (unrenormalized) gap. However, as ω approaches $-\Delta$ from below, the spectral weight for $k=k_F$ diverges as

$$A(\mathbf{k}_F,\omega)\cong\frac{\Delta}{\pi\Gamma}\frac{1}{\sqrt{\omega^2-\Delta^2}}. \tag{A8}$$

As seen in Fig. 13, this square root singularity gives way to a more symmetrically shaped dispersing quasiparticle peak as $\mathbf{k}$ moves away from $\mathbf{k}_F$. However, for $\mathbf{k}$ not too far from the Fermi level, a residual square root singularity at $\omega=-\Delta$ remains. In Fig 14 which shows the dependence of the spectra on disorder, we see that away from the Fermi level the strength of the structure at $\omega=-\Delta$ increases with disorder. In fact one can easily show that when $|\epsilon_k|>\Gamma$, the spectral weight as ω approaches $-\Delta$ varies as $A(\mathbf{k},\omega)\simeq(\Gamma\Delta/\pi\epsilon_k^2)1/\sqrt{\omega^2-\Delta^2}$. Thus in cleaner systems, the anomalous peak at $\omega=-\Delta$ disappears and one has just the expected quasiparticle peak at $\omega=-E_k$.

[1] B. Wells, Z.-X. Shen, A. Matsuura, D. M. King, M. A. Kastner, M. Greven, and R. J. Birgeneau, Phys. Rev. Lett. **74**, 964 (1995).

[2] F. Ronning, C. Kim, D. L. Feng, D. S. Marshall, A. G. Loeser, L. L. Miller, J. N. Eckstein, I. Bozovic, and Z.-X. Shen, Science **282**, 2067 (1998).

[3] T. Valla, A. V. Fedorov, P. D. Johnson, Q. Li, G. D. Gu, and N. Koshizuka, Phys. Rev. Lett. **85**, 828 (2000).

[4] A. Kaminski, J. Mesot, H. Fretwell, J. C. Campuzano, M. R. Norman, M. Randeria, H. Ding, T. Sato, T. Takahashi, T. Mochiku, K. Kadowaki, and H. Hoechst, Phys. Rev. Lett. **84**, 1788 (2000).

[5] A. Damascelli, Z. Hussain, and Z.-X. Shen, Rev. Mod. Phys. **75**, 473 (2003).

[6] E. Abrahams and C. M. Varma, Proc. Natl. Acad. Sci. U.S.A. **97**, 5714 (2000).

[7] J. Giapintzakis, D. M. Ginsberg, M. A. Kirk, and S. Ockers, Phys. Rev. B **50**, 15 967 (1994).
[8] G. Haran and A.D. S. Nagi, Phys. Rev. B **54**, 15463 (1996); **58**, 12 441 (1998); M. L. Kulic and O. V. Dolgov, *ibid.* **60**, 13 062 (1999).
[9] H.-Y. Kee, Phys. Rev. B **64**, 012506 (2001).
[10] D. L. Feng, N. P. Armitage, D. H. Lu, A. Damascelli, J. P. Hu, P. Bogdanov, A. Lanzara, F. Ronning, K. M. Shen, H. Eisaki, C. Kim, and Z.-X. Shen, J.-I. Shimoyama, and K. Kishio, Phys. Rev. Lett. **86**, 5550 (2001).
[11] Y.-D. Chuang, A. D. Gromko, A. Fedorov, Y. Aiura, K. Oka, Yoichi Ando, H. Eisaki, S. I. Uchida, and D. S. Dessau, Phys. Rev. Lett. **87**, 117002 (2001).
[12] P. V. Bogdanov, A. Lanzara, X. J. Zhou, S. A. Kellar, D. L. Feng, E. D. Lu, H. Eisaki, J.-I. Shimoyama, K. Kishio, Z. Hussain, and Z. X. Shen, Phys. Rev. B **64**, 180505 (2001).
[13] A. A. Kordyuk, S. V. Borisenko, T. K. Kim, K. A. Nenkov, M. Knupfer, J. Fink, M. S. Golden, H. Berger, and R. Follath, Phys. Rev. Lett. **89**, 077003 (2002).
[14] A. Kaminski*et al.*, cond-mat/0404385 (unpublished).
[15] H. Eisaki, N. Kaneko, D. L. Feng, A. Damascelli, P. K. Mang, K. M. Shen, Z.-X. Shen, and M. Greven, Phys. Rev. B **69**, 064512 (2004).
[16] L. Zhu, W. A. Atkinson, and P. J. Hirschfeld, Phys. Rev. B **69**, 060503 (2004).
[17] J. E. Hoffman, E. W. Hudson, K. M. Lang, V. Madhavan, and H. Eisaki, Science **295**, 466 (2002); K. McElroy *et al.*, Nature (London) **422**, 592 (2003).
[18] R.S. Markiewicz, Phys. Rev. B **69**, 214517 (2004).
[19] P. W. Anderson, Phys. Rev. Lett. **3**, 328 (1959).
[20] Abrikosov and Gorkov, Zh. Eksp. Teor. Fiz. **39**, 1781 (1960); [Sov. Phys. JETP **12**, 1243 (1961).
[21] W. A. Atkinson, P. J. Hirschfeld, and L. Zhu, Phys. Rev. B **68**, 054501 (2003).
[22] S. M. Quinlan, D. J. Scalapino, and N. Bulut, Phys. Rev. B **49**, 1470 (1994).
[23] M. L. Titov, A. G. Yashenkin, and D. N. Aristov, Phys. Rev. B **52**, 10 626 (1995).
[24] S. M. Quinlan, P. J. Hirschfeld, and D. J. Scalapino, Phys. Rev. B **53**, 8575 (1996).